Calculation of electron-loss-to-continuum cusps: An algebraic approach

J. Burgdörfer,* M. Breinig, S. B. Elston, and I. A. Sellin
University of Tennessee, Knoxville, Tennessee 37966
and Oak Ridge National Laboratory, Oak Ridge, Tennessee 37830
(Received 27 June 1983)

An algebraic approach for evaluation of the bound-free transition form factor $\langle \vec{v}^{\,-} | \exp(i\vec{Q}\cdot\vec{r}) | n,l,m \rangle$ between arbitrary hydrogenic initial states $| n,l,m \rangle$ and continuum final states $| \vec{v}^{\,-} \rangle$ in the low-velocity limit $v \ll Z/n$ is developed. This form factor determines the initial-state dependence of the electron-loss-to-continuum (ELC) cusp in the Born approximation. The method extends the well-known algebraic O(4,2) approach for bound-bound transitions to low-lying continuum states by exploiting the continuity across the ionization limit. A correspondence between scattering states and Rydberg bound states is established using the fact that the Runge-Lenz vector $\vec{A}$ and the velocity vector $\vec{v}$ become collinear near the ionization threshold. The present method takes explicitly into account the dynamical symmetry of the Coulomb field. We use the result for a systematic investigation of the doubly differential cross section and the shape of ELC cusps as a function of the initial state, its binding energy, the target, and the projectile velocity (v_P) within the Born approximation. Comparison is made with recent experimental data from our laboratory for highly charged projectiles. We find qualitative—and sometimes quantitative—agreement with the data.

I. INTRODUCTION

Cross sections for electron emission in inelastic ion-atom collisions show a strong enhancement at electron velocities $\vec{v}_e$ approximately equal to the projectile velocity $\vec{v}_P$. This gives rise to a cusp in the experimentally observed singly differential cross section (SDCS) $d\sigma/dv_e$ for electron emission with velocities $v_e \approx v_P$ into a narrow cone of (semi)angle θ_0 centered about the forward direction. Two different processes contribute to the cusp: target ionization [i.e., electron capture to continuum (ECC)] and projectile ionization [i.e., electron loss to continuum (ELC)]. In both cases, the final electronic state is a near-zero velocity Coulomb wave $| \vec{v}^{\,-} \rangle$ in the rest frame of the projectile. As first discussed by Salin[1] and Macek[2] for ECC, the cusp originates from the singularity in the low-velocity limit of the Coulomb normalization factor (in atomic units)

$$|N(v)|^2 = 2\pi\eta \ , \tag{1}$$

where $\eta = Z_P/v$ and Z_P denotes the (effective) charge of the projectile. In a series of papers, Briggs, Drepper, and Day have shown[3] that a similar singularity occurs for ELC. Their calculation in Born approximation for ionization of a hydrogenic $1s$ projectile state furthermore yields an anisotropic electron distribution, deviating from an isotropic $1/v$ behavior in the projectile rest frame predicted by Eq. (1).

Recent experiments[4,5] have measured the shape of the ELC cusp, characterized by the width [full width at half maximum (FWHM)], the forward-backward asymmetry with respect to the cusp peak, and the total cusp cross section integrated over an arbitrarily chosen interval ($v_P - 0.5 \le v_e \le v_P + 0.5$). For highly charged projectiles having relatively loosely bound L-shell electrons, we have found an almost symmetric cusp with a narrow width in the range $\Gamma = 0.25$–0.3 a.u. nearly independent of v_P, Z_P, and the target. These results differ significantly from corresponding findings for ECC and a theoretical explanation has heretofore not been available. A direct comparison with the calculation for the $1s$ state[3] is not possible for two reasons: In any experiment which does not detect the final charge state of the outgoing projectile in coincidence, the ELC contribution dominates the cusp only if sufficient loosely bound $n = 2$ electrons are available. Furthermore, the Born criterion $Z_P/nv_P \ll 1$ is in most cases studied to date only marginally satisfied for the deeply bound $1s$ state. A systematic theoretical study of the ELC cusp shape as a function of the initial state of the released electron, its binding energy, the projectile velocity, and the target structure was therefore initiated.

The previous calculation[3] for ionization of the $1s$ state in the low-velocity limit has been generalized to arbitrary hydrogenic initial states $| nlm \rangle$ by evaluating the bound-free transition form factor[6]

$$T(n,l,m \to \vec{v},\vec{Q}) = \langle \vec{v}^{\,-} | \exp(i\vec{Q}\cdot\vec{r}) | n,l,m \rangle \tag{2}$$

using a group-theoretical method.

A first suggestion of the possibility of an algebraic treatment of Coulomb excitation taking explicitly into account the dynamical symmetry of the Coulomb field dates back to a paper of Biedenharn[7] in 1961. Since then, rapid progress has been made in calculating matrix elements between hydrogenic bound states for functions in the canonical variables $\vec{r}$ and $\vec{p}$. The algebraic method uses the fact that the hydrogenic bound-state Hilbert space forms an irreducible representation space of the O(4,2) noninvariance

algebra. A comprehensive review of the method has been given by Englefield.[8] In this paper this technique is extended to a calculation of the bound-free transition form factor for low-lying continuum states exploiting the continuity across the ionization limit. Beyond its interesting formal aspects, the present method gives relatively simple closed expressions for the small velocity limit of the transition form factor. For the general case of arbitrary ejection velocities, analytical expressions have been given previously by Omidvar[9] in terms of a series expansion containing an eightfold sum and by Belkić[10] in terms of Appell functions.

The plan of the paper is as following: In Sec. II we briefly review the Born approximation for the triply (TDCS) and doubly differential cross section (DDCS) for projectile ionization in collisions with neutral targets. In Sec. III we express the low-velocity limit of the continuum wave function as a coherent superposition of parabolic Rydberg states $|n',n_1',n_2'm'\rangle$ incorporating the boundary conditions for an incoming (outgoing) Coulomb wave. This result is used in Sec. IV to calculate the bound-free transition form factor as a Rydberg limit $n'\to\infty$ of the bound-bound transition form factor. General symmetry properties and the multipole expansion of the TDCS and DDCS are investigated in Sec. V. In Sec. VI we discuss numerical results for the DDCS and the cusp shape and compare these results with recent experimental data for ELC from our laboratory. In the Appendix, the O(4,2) calculation for the bound-bound transition form factor in hydrogen is briefly sketched. Atomic units are used throughout the paper.

II. FORMULATION OF THE PROBLEM

We consider the ionization of a hydrogenic projectile P in a collision with a neutral target atom T:

$$P^{(Z_P-1)+}+T\to P^{Z_P+}+e+T(?)\ . \tag{3}$$

Since the target final state is not detected in the experiment a sum over all final states has to be performed. The projectile velocity $\vec{v}_P$, parallel to the z axis in the laboratory frame, is assumed to be large compared with the initial orbital velocity of the electron

$$v_P \gg Z_P/n\ . \tag{4}$$

The velocity of the ejected electron in the laboratory frame, v_e, is assumed to match the projectile velocity in both magnitude and direction so that the electron velocity in the projectile rest frame, $\vec{v}$, obeys the inequality

$$|\vec{v}|=|\vec{v}_e-\vec{v}_p| \ll Z_P/n\ . \tag{5}$$

Using the straight-line trajectory impact parameter (IP) formulation, the TDCS for electron emission with velocity v and for simultaneous scattering of the projectile into the laboratory frame solid angle $\Omega_P=(\theta_P,\phi_P)$ is given in Born approximation by[3,11]

$$\frac{d^2\sigma}{d\Omega_P d\vec{v}}=4M_P^2\sum_{k=1}^{2}\frac{1}{Q_k^4}\,|T(n,l,m\to\vec{v},\vec{Q}_k)|^2 S_k(Q_k^2)\ . \tag{6}$$

In Eq. (6), the transverse components $\vec{q}$ of the momentum-transfer vector $\vec{Q}_k=(\vec{q},\gamma_k)$ are given for small $\theta_P \ll 1$ in cylindrical coordinates by

$$\vec{q}=(M_P v_P\theta_P,\phi_P) \tag{7}$$

with M_P the projectile mass (in a.u.). The longitudinal momentum transfer is expressed in terms of the excitation energy of the projectile (ϵ^P) and the target (ϵ_k^T) as

$$\gamma_k=-(\epsilon^P+\epsilon_k^T)/v_P\ . \tag{8}$$

In Eq. (6) a closure approximation[12] has been introduced by considering only two final states for the target. (a) The target remains in its ground state ($\epsilon_{k=1}^T=0$). Then $S_1(Q_1^2)=[Z_T-F(Q_1^2)]^2$ describes the elastic scattering in terms of the atomic form factor F and the charge of the target Z_T; or (b) the target is excited with an average excitation energy $\epsilon_{k=2}^T$ (to be set equal to the ionization potential below). In this case, $S_2(Q_2^2)$ is the incoherent scattering function of the target.

Because of the three approximations assumed in Eq. (6), the following limitations apply to the validity of Eq. (6): The IP method is equivalent to a quantal three-body treatment up to corrections of order $1/\mu$ ($\mu\simeq 10^3$ a.u. the reduced mass of the colliding particles) and only for near-forward scattering ($\theta_P \ll 1$) when the influence of the Coulomb deflection on the electronic transition can be neglected.[13] Both requirements are well satisfied for heavy projectiles in the MeV region. The validity of the closure approximation for target-inelastic processes is often questionable, in particular for describing emission of energetic electrons. In the present case of low-velocity emission, the closure approximation is less critical for two reasons. For light targets, for which target-inelastic processes dominate the projectile ionization, the closure approximation gives reasonable agreement with an explicit summation over excited states[3] in the limit $v \ll 1$. For heavier targets, the target-elastic channel dominates the cross section and the closure approximation for target-inelastic processes becomes less important. Finally, for low-lying continuum states [Eq. (5)] and large projectile velocities [Eq. (4)], the Born approximation is believed to be a reasonable first-order approximation for ionization.[14] In addition to Eq. (4), the Born approximation also requires the interaction strength with the target nucleus to be small, i.e.,

$$Z_T/v_P \ll 1\ . \tag{9}$$

In fact, this requirement is too restrictive because of the electronic screening of the target nucleus. The Born approximation should therefore be applicable to a broader range of collision velocities unless small impact parameters dominate the cross section.

In order to study the magnetic substate dependences, we choose a space-fixed quantization axis along the beam axis ($\hat{v}_P=\hat{z}$) in contrast to the rotational averaging performed in previous ionization calculations for higher angular momentum states.[9,15]

The DDCS is given by an integral over all transverse momenta in Eq. (6):

$$\frac{d\sigma}{d\vec{v}}=\frac{4}{v_P^2}\sum_{k=1}^{2}\int\frac{d^2\vec{q}}{Q_k^4}\,|\,T(n,l,m\rightarrow\vec{v},\vec{Q}_k)\,|^2 S_k(Q_k^2)\ . \tag{10}$$

The DDCS is therefore rotationally symmetric with respect to the $\hat{z}$ axis. Finally, the SDCS for electron emission with velocities $v_e\approx v_P$ into a narrow cone of semiangle θ_0 can be calculated from (10) by integrating the DDCS over the cone solid angle

$$\frac{d\sigma}{dv_e}=v_e^2\int_0^{2\pi}\int_0^{\theta_0}\frac{d\sigma}{d\vec{v}}\sin\theta_e d\theta_e d\phi_e\ . \tag{11}$$

In the experiment, electrons are collected lying in a (approximately) disk-shaped detection volume with diameter $\sim 2v_P\theta_0$ and thickness δv_e determined by the energy resolution of the analyzer. Because in most cases $\delta v_e \ll 2v_P\theta$, the detected cusp shape is close to the singly differential cross section [Eq. (11)] to which we will refer in the following.

III. ANALYTIC CONTINUATION OF THE WAVE FUNCTION ACROSS THE IONIZATION LIMIT

The previous ELC cusp shape analysis for the $1s$ state[3] was performed by calculating the $v\rightarrow 0$ limit of the full transition form factor (valid for arbitrary v). This procedure becomes increasingly complicated for higher principal shells. Therefore, we use an alternative approach based on the continuity across the ionization limit to calculate the small-velocity limit of $T(n,l,m\rightarrow\vec{v},\vec{Q})$ directly without referring to the full transition form factor. The intimate relationship between the density of Rydberg states, the cusp singularity in the low-lying continuum and the continuity across the ionization limit was first discussed by Rudd and Macek.[16]

The key point of the present method is the explicit use of the analyticity of the hydrogenic Schrödinger equation in energy (or in n) to expand low-lying continuum states in terms of high-lying Rydberg states. The expansion coefficients can be found most conveniently by taking into account the dynamical symmetry of the Coulomb field. The O(4) symmetry is connected with an additional constant of motion, the Runge-Lenz vector

$$\vec{A}=\tfrac{1}{2}(\vec{p}\times\vec{L}-\vec{L}\times\vec{p})-Z_P\frac{\vec{r}}{|\vec{r}|} \tag{12}$$

with $\vec{p}$ the linear and $\vec{L}$ the angular momentum. In a classical picture, $\vec{A}$ points from the nucleus to the perihelion of the electronic orbit and determines the orientation the principal axis of the orbit (Fig. 1). $|\vec{A}|$ is proportional to the eccentricity. Cusp states near the ionization limit correspond, classically, to parabolic orbits as the limit of both hyperbolas (continuum states) and ellipses (bound states). As is obvious from Fig. 1, the Runge-Lenz vector is either parallel or antiparallel to the asymptotic velocity of the cusp electron at large separations from the nucleus. More precisely, we find for the $\hat{v}$ component of the Runge-Lenz operator the eigenvalue equation

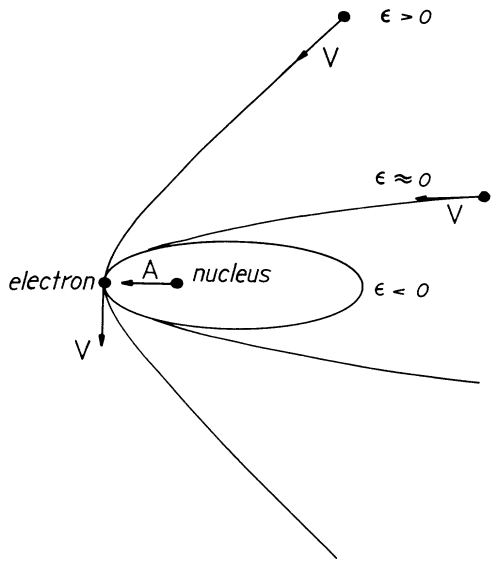

FIG. 1. Classical orbits for the Coulomb problem. For parabolic orbits near the ionization threshold ($\epsilon\approx 0$), the asymptotic velocity at large separations $\vec{v}$ becomes collinear with the Runge-Lenz vector $\vec{A}$.

$$\lim_{v\rightarrow 0}A_v\,|\,\vec{v}^{\,\pm}\rangle=\pm Z_P\,|\,\vec{v}^{\,\pm}\rangle\ . \tag{13}$$

It should be noted that only in the limit $v\rightarrow 0$, the scattering states $|\,\vec{v}^{\,\pm}\rangle$ are eigenstates of A_v.

Since parabolic bound states are eigenstates of a set with

$$A_z\,|\,n',n_1',n_2',m'\rangle=Z_P\frac{n_2'-n_1'}{n}\,|\,n',n_1',n_2',m'\rangle\ , \tag{14}$$

the expansion of the continuum state in terms of parabolic Rydberg states can be found in a simple heuristic way: Comparison of Eqs. (13) and (14) shows that in a coordinate frame Σ_v with z_v parallel to $\vec{v}$, the incoming Coulomb wave $|\,\vec{v}\,\rangle$ can be approximated by parabolic states with quantum numbers $n_1'/n'\simeq 1$ and $n_2'/n'\simeq 0$ for $n'\gg 1$. We therefore choose

$$\lim_{i\eta\rightarrow i\infty}|\,\vec{v}^{\,-}\rangle=e^{i\delta}\lim_{n'\rightarrow\infty}|\,n',\,n_1'=n'-1,\,n_2'=0,\,m'=0\rangle \tag{15}$$

in order to minimize the error in the eigenvalue of the Runge-Lenz operator. The choice of the azimuthal quantum number $m'=0$ follows from

$$\vec{L}\cdot\vec{v}=0 \tag{16}$$

for scattering states.

In Eq. (15) we have rewritten the $v\rightarrow 0$ limit in a more symmetric form by using the analytic continuation of the principal quantum number, n', to the imaginary axis, $i\eta$. Projecting the complex n' plane onto a Rieman sphere of complex numbers,[17] it can be easily seen that the limits $n'\rightarrow\infty$ and $i\eta\rightarrow i\infty$ both converge to the north pole of the sphere where the cusp singularity is located.

The corresponding zero-velocity limit for an outgoing Coulomb wave follows from Eq. (15) by interchanging n_1' and n_2'. The Rydberg limit of the parabolic wave function[18] can be obtained by an asymptotic expansion of the Laguerre polynomials[19] in the limit of large indices ($n_1' \to \infty$) and small arguments ($Z_P r/n' \to 0$) as

$$\lim_{i\eta \to i\infty} \langle \vec{r} \mid \vec{v} \rangle = e^{i\delta} \lim_{n' \to \infty} \left[\frac{Z_P^3}{\pi (n')^4} \right]^{1/2} \times J_0[4Z_p r(1+\cos\tilde{\theta})]^{1/2} . \quad (17)$$

In Eq. (17) J_0 denotes the Bessel function of zeroth order and $\theta = \cos^{-1}(\hat{r}\cdot\hat{v})$. With the use of the standard definition of the parabolic wave functions the relative phase in Eqs. (15) and (17) has to be chosen as $\delta = \arg[\Gamma(1+i\eta)]$. We express the normalization factor of the Rydberg state in a form better suited for continuation across the ionization limit by introducing density of bound states near the ionization threshold $D(\epsilon \to 0^-)$:

$$\lim_{n' \to \infty} \left[\frac{Z_p^3}{\pi (n')^4} \right]^{1/2} = \left[\frac{Z_p}{\pi D(\epsilon = 0^-)} \right]^{1/2} . \quad (18)$$

Notice that the proper density of hydrogenic bound states which correspond to scattering states in the Rydberg limit is proportional to $(n')^4$ rather than $\sim (n')^5$ for the total density of states because of the constraint (16).

Equation (17) can now be transformed to an arbitrarily oriented coordinate frame Σ. If we denote the spherical angles of $\vec{r}$ with respect to Σ by (θ_r, ϕ_r) and those of $\vec{v}$ by (θ_v, ϕ_v), we find

$$\cos\tilde{\theta} = \cos\theta_r \cos\theta_v + \sin\theta_r \sin\theta_v \cos(\phi_r - \phi_v) \quad (19)$$

and Eq. (17) becomes with the help of the addition theorem for Bessel functions,[20]

$$\lim_{i\eta \to \infty} \langle \vec{r} \mid \vec{v}^- \rangle = \left[\frac{Z_p}{\pi D(0^-)} \right]^{1/2} \sum_{m=-\infty}^{\infty} J_m[4Z_p r(1+\cos\theta_r)\cos^2(\theta_v/2)]^{1/2} J_m[4Z_p r(1+\cos\theta_r)\sin^2(\theta_v/2)]^{1/2} e^{im(\phi_r - \phi_v)} . \quad (20)$$

Comparison with the Rydberg limit of parabolic wave functions shows that Eq. (20) can be rewritten as

$$\lim_{i\eta \to i\infty} \mid \vec{v}^- \rangle = e^{i\delta} \lim_{n' \to \infty} \sum_{m=-\infty}^{\infty} \mid n', n_1', n_2', m \rangle e^{-im\phi_v} \quad (21)$$

with

$$n_1'/n' = \cos^2(\theta_v/2) , \quad (22a)$$

$$n_2'/n' = \sin^2(\theta_v/2) . \quad (22b)$$

In Eqs. (22a) and (22b) as in Eq. (15) the identification of the parabolic quantum numbers is accurate only up to corrections of the order $1/n'$. Equation (21) is the desired expansion for the low-velocity continuum function in terms of parabolic Rydberg states.

Only a single combination of parabolic quantum numbers appears determined by the emission angle of the electron [Eq. (22)]. This particularly simple expansion in terms of parabolic states rather than spherical states is an obvious consequence of Wigner's threshold law for an attractive Coulomb field.[21] The wave function immediately above the ionization threshold is a coherent superposition of all partial waves. The wave function [Eq. (21)] contains the leading term of the cusp singularity ($\sim v^{-1/2}$) according to Eq. (1), as can be seen from the continuation of the normalization factor across the ionization limit ($\epsilon \to 0^+$)

$$\left[\frac{Z_p}{\pi D(\epsilon = 0^+)} \right]^{1/2} = \frac{1}{2\pi} \eta^{1/2} . \quad (23)$$

In Eq. (23) $D(\epsilon = 0^+)$ denotes the density of low-lying continuum states. Notice, however, that Eq. (21) does not include higher-order terms in a v expansion [$\sim v^{-1/2}(1 + cv + \cdots)$] exploited in the fitting parameter approach used by Meckbach *et al.*[22] The small-velocity limit is therefore expected to be valid only in the immediate vicinity of the cusp singularity. Deviations must be expected in the tails of the cusp shape.

It should be remarked that the expansion (21) can also be derived in a more rigorous way by using the SU(2)×SU(2) pseudospin formulation[23] of the hydrogenic invariance group O(4) and the classical limit of the Wigner rotation matrices.[24]

IV. THE BOUND-FREE TRANSITION FORM FACTOR

With the use of the results of the preceding section, the low-velocity limit of the bound-free transition form factor [Eq. (2)] can be expressed as the Rydberg limit of the bound-bound transition form factor

$$\lim_{i\eta \to i\infty} T(n,l,m \to \vec{v}, \vec{0}) = e^{-i\delta} \sum_{m'=-\infty}^{\infty} e^{im'\phi_v} \times \lim_{n' \to \infty} \langle n', n_1', n_2', m' \mid e^{i\vec{Q}\cdot\vec{r}} \mid n,l,m \rangle . \quad (24)$$

Notice that Eq. (24) contains the directional information of three vectors (Fig. 2): the beam velocity $\vec{v}_P$ defines the quantization axis of the initial state $\mid n,l,m \rangle$, $\vec{Q}$ describes the orientation of the momentum transfer vector during the collision and determines in the present case of small-angle scattering the projectile scattering angle according to Eq. (7), and finally, $\vec{v}$ defines the direction of the emitted electron [compare Eq. (24)]. For an investigation of the magnetic substate dependence of the TDCS and DDCS we have to keep track of all these angular dependences in contrast to the rotational averaging employed in previous calculations for ionization of higher

angular momentum states.[9,15] The right-hand side of Eq. (24) can be evaluated most conveniently in a coordinate frame Σ_Q with z_Q parallel to $\vec{Q}$. The initial state can be transformed into the Σ_Q frame with help of the rotational matrix[25] $D^l_{m,m''}$:

$$|n,l,m\rangle = \sum_{m''=-l}^{l} D^l_{m,m''}(-\phi_Q,\theta_Q)\,|n,l,m''\rangle \tag{25}$$

with $\Omega_Q=(\theta_Q,\phi_Q)$ the spherical angle of $\vec{Q}$ as seen in the space-fixed coordinate frame with the z axis parallel to $\vec{v}_P$. The corresponding transformation for the final state is given by Eqs. (21) and (22) with $\Omega_v(Q)=(\theta_v(Q),\phi_v(Q))$ the spherical angles of $\vec{v}$ in Σ_Q (Fig. 2). $\Omega_v(Q)$ can be expressed in terms of the spherical angles of $\hat{Q},\Omega_Q$, and $\hat{v},\Omega_v=(\theta_v,\phi_v)$ in the space-fixed frame with help of the addition theorem for spherical angles [compare Eq. (19)]. Since $\exp(i\vec{Q}\cdot\vec{r})$ possesses rotational symmetry around the z_0 axis, we can rewrite Eq. (24) as

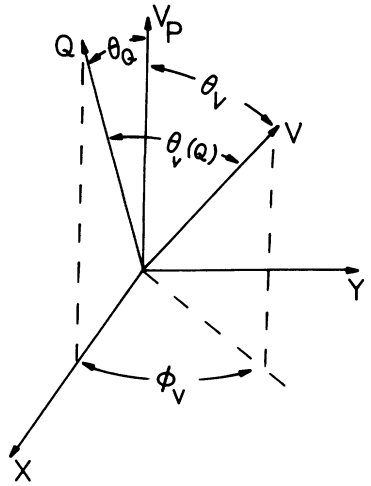

FIG. 2. Geometric relationship between the projectile velocity $\vec{v}_P$ (chosen as the z axis of the space-fixed frame), the momentum transfer vector $\vec{Q}$ in the x-z collision plane, and electron velocity $\vec{v}$. $\theta_v(Q)$ is the polar angle of $\vec{v}$ in the rotated frame Σ_Q with $\vec{Q}$ chosen as z_Q axis.

$$\lim_{i\eta\to i\infty} T(n,l,m\to\vec{v},\vec{Q}) = e^{-i\delta}\sum_{m''=-l}^{l} D^l_{m,m''}(-\phi_Q,\theta_Q,-\phi_v(Q)) \lim_{n'\to\infty}\langle n',n'_1,n'_2,m''\,|\,e^{iQz_Q}\,|\,n,l,m''\rangle \tag{26}$$

with $n'_1/n'=\cos^2[\theta_v(Q)/2]$ and $n'_2/n'=\sin^2[\theta_v(Q)/2]$.

For a further evaluation it is convenient to transform Eq. (26) into a representation involving only parabolic eigenfunctions by using the pseudospin coupling relation[26]

$$|n,l,m''\rangle = \sum_{n_1,n_2=0}^{n-1-|m''|}\langle l,m''\,|\,jjm_1m_2\rangle(-1)^{j+m_1}\,|\,n,n_1,n_2,m''\rangle \tag{27a}$$

with

$$m_1+m_2=m'' , \tag{27b}$$

$$m_1-m_2=n_1-n_2 , \tag{27c}$$

$$j=(n-1)/2 , \tag{27d}$$

and

$$n=n_1+n_2+|m''|+1 . \tag{27e}$$

Inserting Eq. (27) in Eq. (26) gives

$$\lim_{i\eta\to in\infty} T(n,l,m\to\vec{v},\vec{Q}) = e^{-i\delta}\sum_{m''=-l}^{l} D^l_{m,m''}(-\phi_Q,\theta_Q,-\phi_v(Q)) \sum_{n_1,n_2=0}^{n-1-|m''|}(-1)^{j+m_1}\langle l,m''\,|\,j_1j_1m_1m_2\rangle \times \lim_{n'\to\infty}\langle n',n'_1,n'_2,m''\,|\,e^{iQz_Q}\,|\,n,n_1,n_2,m''\rangle . \tag{28}$$

The problem is thus reduced to a calculation of the bound-bound transition form factor between arbitrary parabolic states. As is well known, the latter can be calculated in a purely algebraic way exploiting the fact that hydrogenic bound states form an irreducible representation space of the O(4,2) noninvariance algebra. A comprehensive discussion of this approach can be found in Ref. 8. In the Appendix we briefly summarize the major results adopted to our present notation.

In the following we extend this approach to low-lying continuum final states by calculating the Rydberg limit of Eq. (A4). We perform an asymptotic expansion for $n',n'_1,n'_2\to\infty$ subject to the constraint Eq. (22). The leading order behaves as $(n')^{-2}$ as required by the continuity across the ionization limit [compare Eq. (18)]. After a lengthy but straightforward calculation we arrive at

$$\lim_{n'\to\infty}\langle n',n_1',n_2',m''\,|\,e^{iQz_Q}\,|\,n,n_1,n_2,m''\rangle$$

$$=(-1)^{n_1+n_2}\frac{K}{2Z_P[D(0)]^{1/2}(|m''|!)^2B}\left[\frac{(n_1+|m''|)!(n_2+|m''|)!}{n_1!n_2!}\right]^{1/2}$$

$$\times\left[\frac{\sin[\theta_v(Q)]}{2}\right]^{|m''|}C^{2+|m''|}\exp\left[-\frac{C}{2}\{1+i\cos[\theta_v(Q)]Kn\}\right]$$

$$\times\left[\frac{1+iKn}{1-iKn}\right]^{n_1-n_2}\{\{2Kn^2-2in\cos[\theta_v(Q)]+iB(n_1-n_2)\}$$

$$\times\,{}_1F_1(-n_1,|m''|+1,C\cos^2[\theta_v(Q)/2])\,{}_1F_1(-n_2,|m''|+1,C\sin^2[\theta_v(Q)/2])$$

$$+iB[n_2\,{}_1F_1(-n_1,|m''|+1,C\cos^2[\theta_v(Q)/2])\,{}_1F_1(-(n_2-1),|m''|+1,C\sin^2[\theta_v(Q)/2])$$

$$-n_1\,{}_1F_1(-(n_1-1),|m''|+1,C\cos^2[\theta_v(Q)/2])\,{}_1F_1(-n_2,|m''|+1,C\sin^2[\theta_v(Q)/2])]\}\,. \tag{29}$$

In Eq. (29), we have substituted the density of states [Eq. (18)] and the following abbreviations:

$$K=Q/Z_P\,, \tag{30a}$$

$$B=(1+n^2K^2)\,, \tag{30b}$$

$$C=4n/B\,. \tag{30c}$$

Equations (28) and (29) are the final results for the transition factor from arbitrary initial n,l,m to low-velocity continuum states. Inserting Eqs. (28) and (29) into (6) yields the TDCS in closed form. For the DDCS, a one-dimensional numerical integration has to be performed according to Eq. (10). The algebraic evaluation of the transition form factor yields a relatively compact and transparent expression as compared to a direct integration[9] in coordinate space. Furthermore, our expression contains the full information about the relative orientation of $\vec{Q}$, $\vec{v}$, and $\vec{v}_P$ in contrast to rotational averaging in Ref. 9. The validity of the present approach is limited to the low ejection velocity region. Deviations must be expected when the characteristic wavelength of the initial and final states become of comparable magnitude. We find therefore $v\ll Z_P/n$ [Eq. (5)] as a criterion for the applicability of Eqs. (28) and (29). This criterion is fulfilled for experimental ELC cusp shapes for highly charged ions and low-lying n states with a typical half-width[5] $\Gamma/2\approx 0.15$ a.u. in velocity space.

V. SYMMETRIES OF THE ELECTRON DISTRIBUTION

We investigate now the symmetry properties of the final electron distribution. Most of the desired relations can be derived without using the explicit expression Eq. (29).

Applying the parity operator P ($\vec{r}\to-\vec{r}$) to the initial and final states we find

$$\langle-\vec{r}\,|\,\vec{v}^{\,\pm}\rangle=\langle\vec{r}\,|\,-\vec{v}^{\,\pm}\rangle\,, \tag{31a}$$

$$\langle-\vec{r}\,|\,n,l,m\rangle=(-1)^l\langle\vec{r}\,|\,n,l,m\rangle\,, \tag{31b}$$

and consequently, for the transition form factor

$$\langle\vec{v}^{\,-}\,|\,e^{i\vec{Q}\cdot\vec{r}}\,|\,n,l,m\rangle=(-1)^l\langle-\vec{v}^{\,-}\,|\,e^{-i\vec{Q}\cdot\vec{r}}\,|\,n,l,m\rangle\,. \tag{32}$$

Therefore, both the TDCS and DDCS are invariant under simultaneous inversion of $\vec{v}$ and $\vec{Q}$ because of

$$|\,T(n,l,m\to\vec{v},\vec{Q})\,|^2=|\,T(n,l,m\to-\vec{v},-\vec{Q})\,|^2\,. \tag{33}$$

This symmetry relation, which holds for arbitrary v, has only little practical importance because it does not correspond to a symmetry operation for the electronic distribution for a *fixed* beam direction.

More relevant symmetry relations can be derived by using the fact that the low-velocity limit of the continuum wave function [Eq. (17)] is, except for the irrelevant phase factor $e^{i\delta}$, real.

We consider the TDCS first, for which the symmetry is determined by $|\,T(n,l,m\to\vec{v},\vec{Q})\,|^2$. We choose a x-z scattering plane spanned by $\vec{Q}$ and $\vec{v}_p$ ($\phi_0=0$, see Fig. 2). The transition operator $e^{i\vec{Q}\cdot\vec{r}}$ is therefore invariant under plane reflections Π_y: $y\to-y$. We furthermore choose as initial states eigenstates of both Π_y and the complex conjugation operator $\tilde{K}$ with eigenvalues ±1:

$$|\,n,l,m^{\pm}\rangle=\frac{1}{[2(1+\delta_{m,0})]^{1/2}}\times[\,|\,n,l,m\rangle\pm(-1)^m\,|\,n,l,-m\rangle] \tag{34}$$

($m^+=0,1,\ldots,l;m^-=1,2,\ldots,l$). Inserting Eq. (34) into Eq. (32) and using the reality of the $v\to0$ continuum state we find

$$\langle \vec{v}^{\,-} | e^{i\vec{Q}\cdot\vec{r}} | n,l,m^{\pm}\rangle = (-1)^l \langle -\vec{v} | e^{-i\vec{Q}\cdot\vec{r}} | n,l,m^{\pm}\rangle = \pm(-1)^l e^{-2i\delta} (\langle -\vec{v}^{\,-} | e^{i\vec{Q}\cdot\vec{r}} | n,l,m^{\pm}\rangle)^* . \quad (35)$$

Consequently, the TDCS is invariant under the transformation $\vec{v} \to -\vec{v}$ for a *fixed momentum transfer* $\vec{Q}$, i.e.,

$$|T(n,l,m^{\pm} \to -\vec{v},\vec{Q})|^2 = |T(n,l,m^{\pm} \to \vec{v},\vec{Q})|^2 . \quad (36)$$

The transformation properties with respect to rotations can be specified by a decomposition into spherical tensor components ρ_M^L. Explicit expressions can be found by expanding the angular dependences in Eqs. (28) and (29) in terms of spherical harmonics. We omit here the very large expressions for $\rho_m^L(n,l,m^{\pm};q)$. The general feature of the angular distribution can be determined very easily, however, by noting that, except for an irrelevant phase factor, the highest power in $\cos\theta_v$ (or $\sin\theta_v$) in (29) is given by n, irrespective of the quantum numbers (l,m). Combining this with the symmetry relation [Eq. (36)], we find for the triply differential cross section for ELC from an initial state $|n,l,m^{\pm}\rangle$ in Born approximation the expansion

$$\frac{d^2\sigma}{d\theta_P d\vec{v}} = \sum_{\substack{L=0 \\ (\text{even})}}^{2n} \sum_{M^+=0}^{L} \rho_{M^+}^L(n,l,m^{\pm};q) Y_L^{M^+}(\theta_v,\phi_v) \quad (37)$$

with an x-z plane as scattering plane ($\phi_P = 0$). The expansion coefficients ρ_M^L depend on θ_P via q [Eq. (7)]. The spherical harmonics $Y_L^{M^+}$ ($M^+ = 0,1,\ldots,L$) are defined in accordance with Eq. (34). Only even L contribute to Eq. (37) because of the even parity of the electron distribution.

As an important result we find that *the maximum degree of anisotropy $L_{\max} = 2n$ is determined by the principal quantum number rather than by the angular momentum l.* We note that terms in (37) with $L - M^+$ odd are antisymmetric with respect to Π_z. The TDCS for ELC in Born approximation is therefore, in general, forward-backward asymmetric.

The symmetries of the DDCS are according to (10) determined by the expression

$$\int_0^{2\pi} d\phi_Q |T(n,l,m \to \vec{v},\vec{Q})|^2 \quad (38)$$

which possesses rotational symmetry with respect to the z axis. In this case only $M^+ = 0$ components contribute and the multipole expansion becomes

$$\frac{d\sigma}{d\vec{v}} = \frac{1}{v} \sum_{\substack{L=0 \\ (\text{even})}}^{2n} a_L(n,l,|m|) P_L(\cos\theta_v) \quad (39)$$

with expansion coefficients a_L depending only on the absolute magnitude of m. In Eq. (39) we have explicitly displayed the v dependence originating from the normalization factor (23). In the following section, we will present numerical results for the DDCS in terms of the isotropic part a_0 and the anisotropic coefficients

$$\beta_L = a_L/a_0 . \quad (40)$$

Within the Born approximation, for an arbitrary initial state $|n,l,m\rangle$ the low-velocity limit of the DDCS is symmetric with respect to both inversions ($\vec{v} \to -\vec{v}$) and plane reflections ($v_z \to -v_z$) and shows no forward-backward asymmetry in contrast to the TDCS. As discussed in the next section, the singly differential cross section $d\sigma/dv_e$ shows a slight forward-backward asymmetry. This is, however, only due to the kinematics of the transformation to the laboratory frame.

In the special case $n = 1$, Eq. (39) reveals the result previously given by Briggs and Day.[3] The selection rule $L \leq 2n$ is the origin of their findings that, although all partial waves contribute to the scattering amplitude, only zeroth- and second-order multipoles appear in the DDCS for the $1s$ initial state.

It should be noted that the results presented in this section were based on the well-defined parity of the spherical states $|n,l,m\rangle$. An analogous investigation for parabolic initial states $|n,n_1,n_2,m\rangle$ yields also contributions with L odd and consequently a forward-backward asymmetry in the DDCS. This could have significance for convoy electron production in solids when the emitted electron originates from ELC for a coherently excited state (e.g., a parabolic state)[27] near the surface.

VI. NUMERICAL RESULTS

In this section, we present numerical results for the DDCS and the cusp shape in the SDCS, $d\sigma/dv_e$. Of particular interest is the width Γ (FWHM) in velocity of the cusp. We restrict ourselves in the following to initial states of the projectile with $n \leq 2$. For many-electron projectiles we have used hydrogenic wave functions with effective charges for the initial and the final states[28] chosen in accordance to the Slater screening parameters. In our investigations of m-substance dependences, we consider only orbital-angular-momentum states neglecting spin-orbit mixing. Calculations have been made for three different targets (hydrogen, helium, and argon) in order to study the influence of the target structure on the electron distribution. For hydrogen, the scattering functions $F(Q_1^2)$ and $S_2(Q_2^2)$ can be calculated exactly.[12] For helium, we use an analytical approximation[29] reproducing the results of a configuration interaction calculation tabulated by Hubbell *et al.*[30] within a few percent. For argon, we take the tabulated data[30] from a nonrelativistic Hartree-Fock calculation.

A. DDCS

The results for the DDCS for ionization of $He^+(n,l,m)$ on hydrogen are displayed in Figs. 3–5. The isotropic term $a_0(n,l,m)$ (Fig. 3) is identical for all $n = 2$ states within the graphical accuracy of the logarithmic scale. A weak l dependence has also been found by Omidvar and Kyle[31] for the total ionization cross section. The weak l dependences emphasizes the influence of the dynamical symmetry of the Coulomb field. For the deeply bound $1s$ electron $a_0(1s)$ is almost 1 order of magnitude smaller. The n dependence for a_0 is much stronger than for the to-

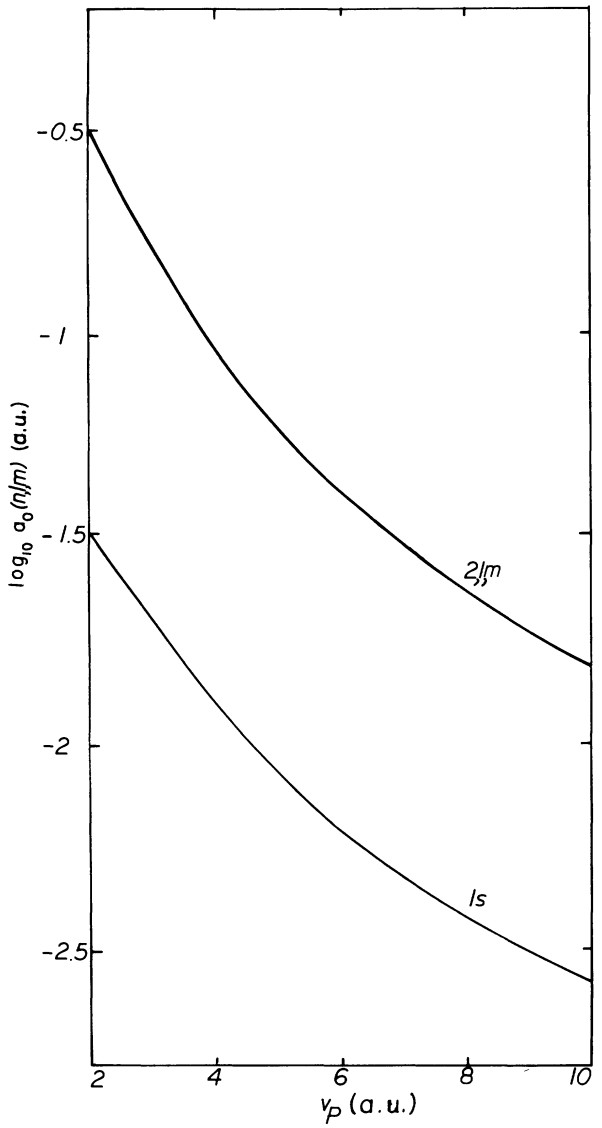

FIG. 3. $\log a_0(n,l,m)$ for ELC of $He^+(n,l,m)$ on H as a function of projectile velocity v_P. For all $n=2$ substates, $\log a_0(2,l,m)$ is identical within the graphical accuracy.

tal ionization cross section.[31] This result indicates that loosely bound electrons, if available in the projectile, strongly dominate the ELC cusp spectrum in agreement with experimental data.[5] The v_P dependence of a_0 for projectile velocities $v_P \gg 1$ scales roughly as v_P^{-2} in accordance with the velocity dependence of the total ionization cross section. The second-order anisotropy coefficients β_2 are displayed in Fig. 4. At large v_P, for all $n=2$ states $|\beta_2|$ is considerably larger than for the $1s$ state. L-shell electrons are emitted highly anisotropically. For the $2s$ and $2p_{\pm 1}$ states the energy dependence of β_2 is similar to that of the $1s$ state describing an electron emission preferentially perpendicular to $\hat{v}_P$ in the limit $v_P \gg 1$. An opposite behavior can be observed for the $2p_0$ initial state: β_2 increases to large positive values $\lesssim 1.7$ approaching almost the positive-definiteness limit $(-1 \le \beta_2 \le 2)$. The emission takes place preferentially parallel or antiparallel to $\hat{v}_P$.

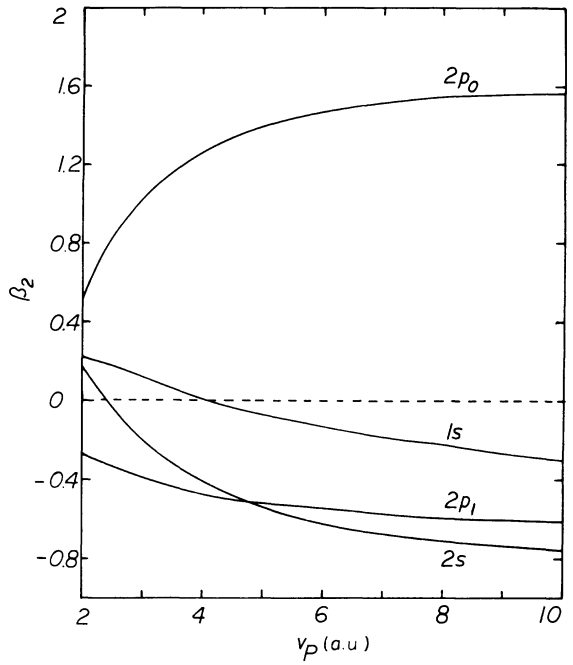

FIG. 4. Second-order anisotropy coefficient $\beta_2(n,l,m)$ for ELC of $He^+(n,l,m)$ on H as a function of projectile velocity v_P.

Since $L_{max}=2n$ for the $n=2$ states there are also fourth-order anisotropy contributions β_4 shown in Fig. 5. The presence of β_4 can introduce additional local minima in the electron distributions near $\theta_v \approx \pi/4$ and $\theta_v \approx 3\pi/4$. As was the case for β_2, values of β_4 also differ significantly for the $2p_0$ state from those for $2s$ and $2p_{\pm 1}$. The entirely different anisotropy for the $2p_0$ state can be traced to its odd Π_z symmetry.[32] For β_4 the positive-definiteness limit is given by $-1 \le \beta_4 \le \frac{7}{3}$.

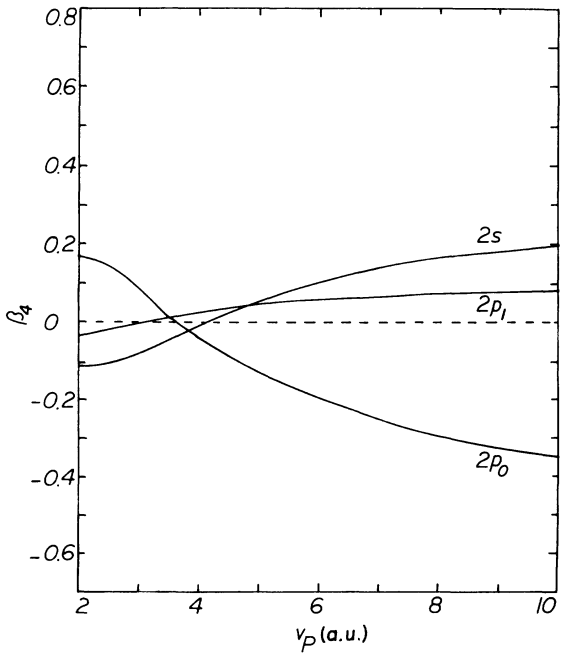

FIG. 5. Fourth-order anisotropy coefficient $\beta_4(n,l,m)$ for ELC of $He^+(n,l,m)$ on H as a function of projectile velocity v_P.

We have found qualitatively similar results for the DDCS when varying Z_P (which determines the initial binding energy of the released electron) and the target. This indicates that the gross feature of the DDCS are primarily determined by the initial state.

B. Cusp shape

According to Eq. (11) the SDCS, $d\sigma/dv_e$, can be calculated from the DDCS by integration over all emission angles $\theta_e \leq \theta_0$ in the laboratory frame lying within the cone angle θ_0. It is therefore necessary to transform the angular distribution in the projectile frame given by Eq. (39) into the laboratory frame with help of the relation

$$\tan\theta_e = \frac{\sin\theta_v}{v_P/v + \cos\theta_v} . \tag{41}$$

Because of the azimuthal symmetry of Eq. (39), the ϕ_e integration in (11) is trivial. The θ_e integration can be performed for all Legendre polynomials P_L leading to cumbersome expressions (especially for high L) not given here. A detailed discussion of the transformation can be found in Ref. 3.

Figure 6 shows the resulting cusp shape in $d\sigma/dv_e$ for the ionization process $He^+(n,l,m)+H \rightarrow He^{2+}+H(?)$ at $v_P=10$ ($\theta_0=3\times10^{-2}$ rad) for different initial states. All cross sections are normalized to unity at the peak position $v_e=v_P$. An important conclusion is that ELC cusps are narrow compared with the cusp for isotropic electron emission (Dettmann shape[33]) also shown in Fig. 6. The Dettmann shape yields a linewidth $\Gamma=\frac{3}{2}\theta_0 v_P=0.45$. We find $\Gamma(1s)=0.3$, $\Gamma(2p_{\pm1})=0.23$, and $\Gamma(2s)=0.2$. The very small linewidth for these states is a consequence of their large negative anisotropy coefficient β_2. The preferred transverse electron emission narrows the longitudinal distribution which basically determines the shape of $d\sigma/dv_e$. For all cusps we observe a slight forward-backward asymmetry with respect to the peak position v_P. This asymmetry is purely kinematic in origin stemming from the fact that for a given θ_0 the detection volume increases as $\sim(v_e\theta_0)^2$ with the laboratory frame velocity.

The $2p_0$ initial state shows at high projectile velocities an inverted cusp which is linked with its odd Π_z symmetry.[32] Figure 7 shows the dip in the ELC spectrum for $He^+(2p_0)$ projectiles on different targets with projectile velocity $v_P=4$. All cross sections are normalized to unity at $v_e=v_P+0.1$ in order to facilitate the comparison. The existence of the dip is obviously independent of the target. The minimum of $d\sigma/dv_e$ at $v_e=v_P$ is proportional to γ_k^2 ($k=1,2$) and therefore sensitive to the target structure. For light targets (hydrogen and helium) the major contribution to the ionization cross section originates from target-inelastic processes ($k=2$). The value $(d\sigma/dv_e)_{v_e=v_P}$ is then (approximately) proportional to γ_2^2 and the dip is less pronounced for He than for H targets because of the larger ionization energy in He [compare Eq. (8)]. The deepest "valley" occurs for argon because for heavier targets the elastic channel ($\epsilon_1^T=0$) with a small γ_1^2 gives the leading contribution to the cross section. For the same reason, the uncertainties introduced by the closure approximation become less important for heavier targets. On the other hand, the dominance of the elastic

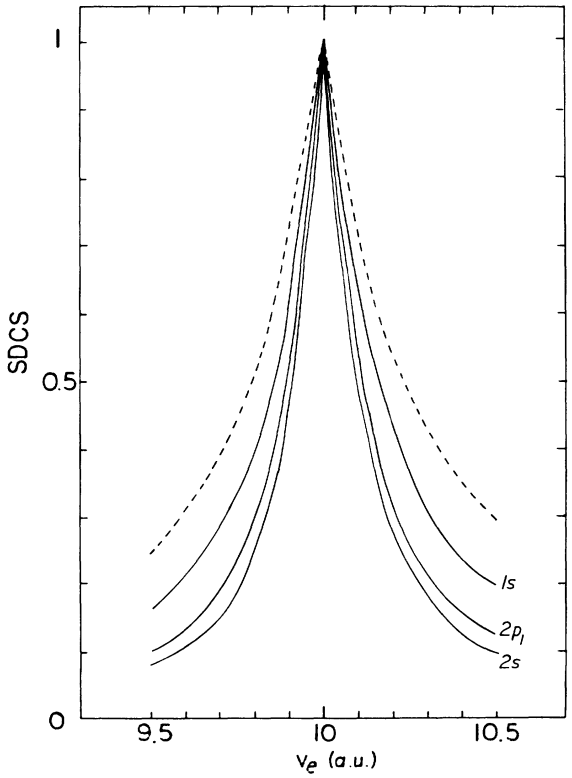

FIG. 6. Normalized singly differential cross section $d\sigma/dv_e$ for ELC of $He^+(n,l,m)$ on H at $v_P=10$ a.u. ($\theta_0=3\times10^{-2}$ rad); — — —, cusp shape for isotropic electron emission.

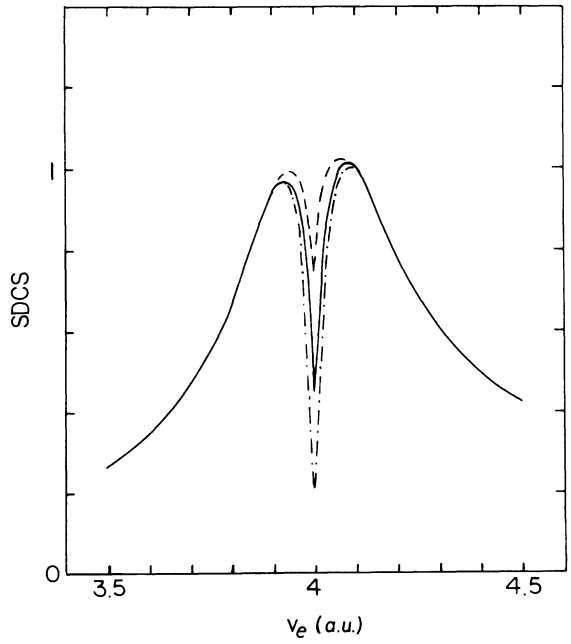

FIG. 7. Cusp inversion for ELC of $He^+(2p_0)$ at $v_P=4$ a.u. ($\theta_0=3\times10^{-2}$ rad) and different targets: ——, hydrogen; — — —, helium; —·—, argon.

channel indicates that small impact parameters contribute considerably to the ELC cross section. Since the screening of the target nucleus is incomplete at small impact parameters, the interaction strength [Eq. (9)] cannot be assumed to be small, and the major limitation on the accuracy arises from the Born approximation itself. The dip can be understood as a simple consequence of the large positive anisotropy β_2 (compare Fig. 4). The electron emission from the $2p_0$ state shows a preferred longitudinal emission which broadens the shape to such an extent that the central peak is inverted.

In an experiment without selective preparation of a particular initial state, $d\sigma/dv_e$ is given by an incoherent superposition of cusp contributions from $1s$, $2s$, and $2p_{\pm 1}$ states and the dip contribution from the $2p_0$ state. Figure 8 shows averaged cusp shapes for a statistically populated $2p$ state, $\sigma_{2P}=(\sigma_{2p,0}+2\sigma_{2p,1})/3$, and an $n=2$ level, $\sigma_2=(\sigma_{2s}+\sigma_{2p})/2$, with equal population in the s and the p states. The dip contribution of the $2p_0$ state broadens the $2p$ cross section to $\Gamma_{2p}=0.57$. The very narrow $2s$ cusp reduces the effective $n=2$ linewidth to an averaged value $\Gamma_2=0.29$. For few-electron projectiles we therefore expect an appreciably narrowed cusp whenever $2s$ electrons are present. This is in good agreement with data for highly charge few-electron projectiles.[5]

The dependence of the cusp width Γ as a function of the effective charge Z_P (i.e., the binding energy) is displayed in Figs. 9 and 10. Only the ground state shows

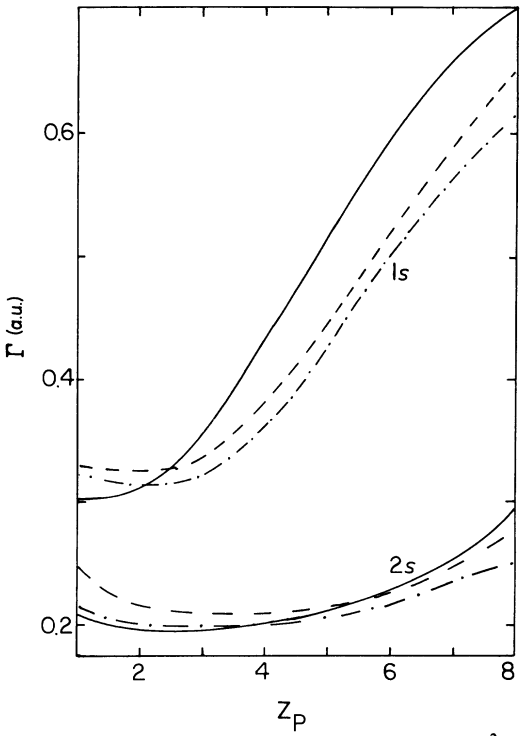

FIG. 9. Cusp width Γ at $v_P=10$ a.u. ($\theta_0=3\times10^{-2}$ rad) as a function of the projectile charge Z_P for $1s$ and $2s$ initial states and different targets: ——, hydrogen; — — —, helium; —·—, argon.

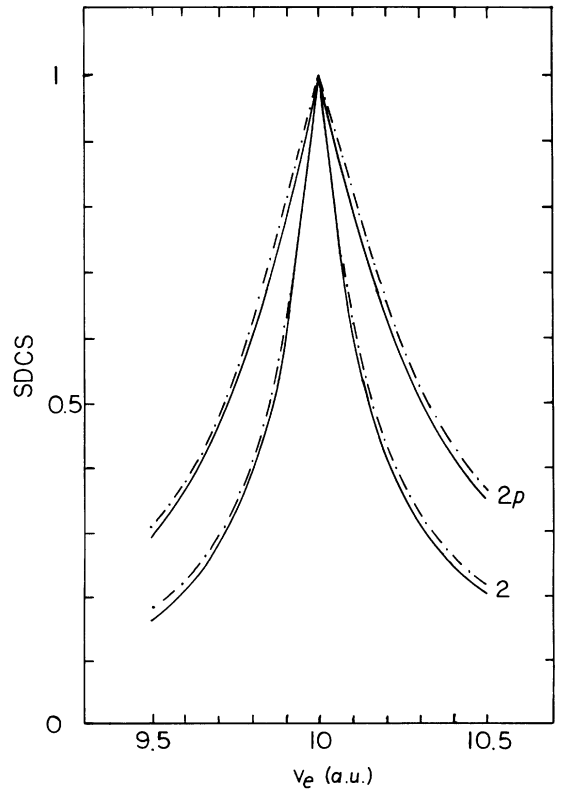

FIG. 8. Singly differential ELC cross section $d\sigma/dv_e$ averaged over all substates of $2p$ and all $n=2$ states (see text) for $He^+(n,l,m)$ at $v_P=10$ a.u. ($\theta=3\times10^{-2}$ rad). Target: ——, hydrogen; —·—, argon.

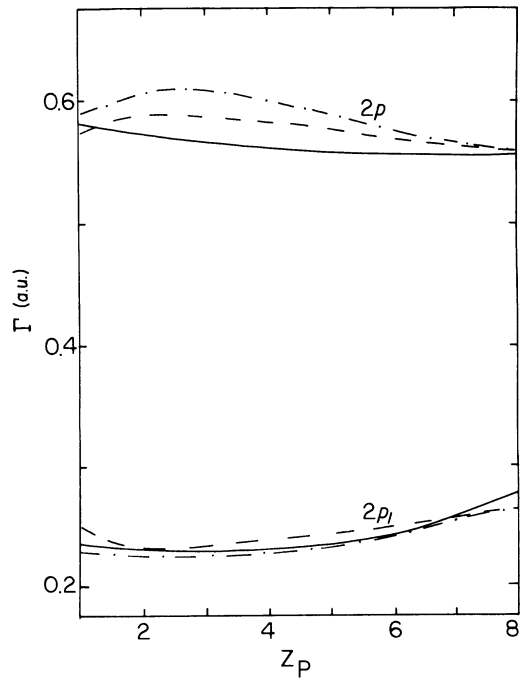

FIG. 10. Cusp width Γ as a function of the projectile charge Z_P for $2p_1$ and averaged $2p$ states. Notation and parameters as in Fig. 9.

a drastic increase of Γ by a factor of 2.5 between $Z_p=1$ and $Z_P=8$. For $n=2$ states, Γ is remarkably insensitive with respect to a variation of the binding energy within a factor 64. The width of the $2s$ and $2p_{\pm1}$ states is confined within the interval $0.2\leq\Gamma\leq0.3$ and for the $n=2$ average, not shown in Fig. 10, we find $\Gamma_2\lesssim0.35$. This agrees, qualitatively, with experimental findings. It is furthermore obvious from Figs. 9 and 10 that the target structure has only little influence on Γ. The slight decrease of Γ for heavier targets (in particular, for the $1s$ state and at large Z_P) is in part due to the increasing importance of the elastic channel which leads, in most cases, to a narrowing of the cusp.

The projectile-velocity dependence of Γ is shown in Figs. 11 and 12 for different projectile effective charges Z_P and for different targets. The cusp width Γ increases, in general, considerably more slowly than $\sim v_P$ predicted for the Dettmann shape. The increase of Γ with v_P is, like the apparent asymmetry, primarily a kinematic effect originating from the increasing detection volume. The enhanced transverse anisotropy for $v_P\rightarrow\infty$ partially compensates for the kinematic broadening. For the $2s$ state (Fig. 12), Γ becomes almost velocity independent over a wide range of velocities. Only the Γ_{2p} increases almost linearly with v_P. The target structure as well as the binding energy have only little influence upon the projectile velocity dependence of Γ.

For the SDCS maximum $[d\sigma/dv_e]_{v_e=v_P}$ a kinematic correction to the v_P dependence in Born approximation (v_P^{-2}) can be expected. For the Dettmann shape the correction factor is $\sim v_P$. Figure 13 shows $[d\sigma/dv_e]_{v_e=v_P}$ as a function of $1/v_P$ for the reaction $He^+(n,l,m)+H$. We find good agreement with a linear behavior for $1/v_P\rightarrow0$ as predicted for an isotropic cusp although the angular distribution is in fact highly anisotropic.

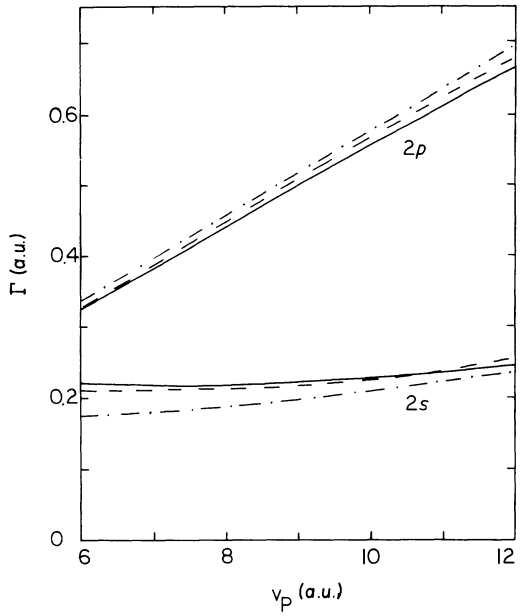

FIG. 12. Cusp width Γ_{2s} and Γ_{2p} as a function of the projectile velocity for $Z_P=6$, notation as in Fig. 11.

The results for the cusp width hold, of course, only for states showing a regular cusp ($1s,2s,2p_{\pm1},2p$). For a $2p_0$ initial state, we find with $v_P\rightarrow\infty$ complete cusp inversion and the electron distribution becomes very broad.

C. Comparison with experiment

A quantitative comparison of the present results with the experiment is meaningful only if the following re-

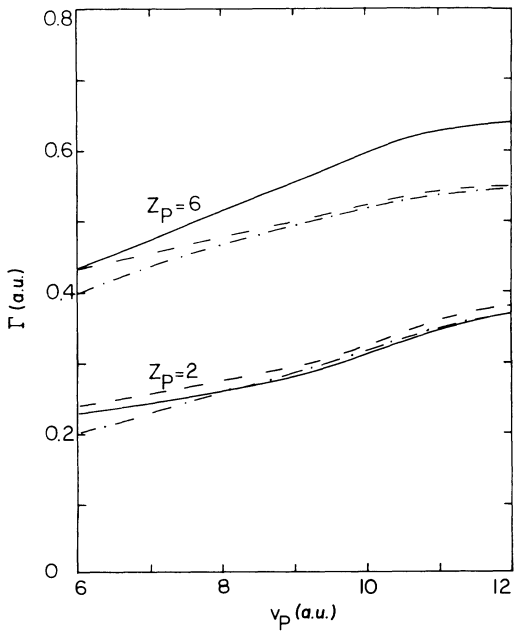

FIG. 11. Cusp width Γ_{1s} as a function of the projectile velocity v_P for different Z_P and targets: ——, hydrogen; — — —, helium; —·—, argon; ($\theta_0=3\times10^{-2}$ rad).

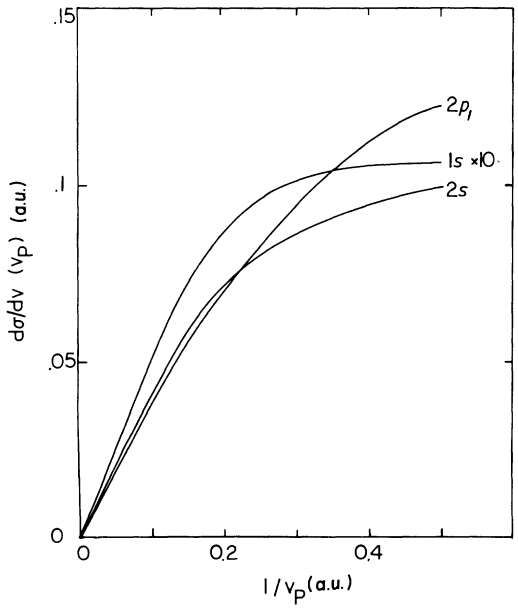

FIG. 13. Singly differential ELC cross section at the matching velocity, $(d\sigma/dv_e)_{v_e=v_P}$, for $He^+(n,l,m)$ on H as a function of the inverse projectile velocity; $\theta_0=3\times10^{-2}$ rad. Cross sections for $1s$ are multiplied by 10.

quirements for the data are met:

(a) the projectile velocity is large compared to the orbital velocity of the released electron [Eq. (4)];

(b) the initial state can be approximated by a hydrogenic wave function without serious error; and

(c) additional charge-transfer contributions (ECC) can be neglected. Most of the data taken so far for highly charged projectiles in our laboratory satisfy these requirements only marginally. An exceptional case are the cusp data for O^{5+}. The large electron-loss cross section for the loosely bound $2s$ electron permits an almost "pure" ELC measurement without significant ECC contribution and without the need for performing a coincidence experiment. The $2s$ state of the Li-like configuration can be described by a hydrogenic wave function with an effective charge $Z_{P,\text{eff}}=6.3$ to a reasonable degree of approximation. The deviation from the asymptotic charge seen by the ionized electron at large distances, $Z_{P,\text{asym}}=6$ is only $\approx 5\%$. For the experimental data in the region $7 \leq v_P \leq 12$ with $v_P/v_{\text{orbital}} \gtrsim 2$ the Born approximation should give a rough estimate for the ELC cross section.

Figure 14 displays the ELC cusp width for O^{5+} on argon. The calculation includes, besides the dominant $2s$ cross section ($\approx 90\%$), the smaller contributions of the two $1s$ electrons ($\approx 10\%$) also described by hydrogenic orbitals with the Slater value $Z_{P,\text{eff}}=7.65$. The linewidth is found to be much smaller than predicted for an isotropic cusp, also shown in Fig. 14, and in good agreement with our data. This result strongly emphasizes the importance of the large transverse anisotropy as a source of the narrowing and of the weak v_P dependence of Γ observed in ELC experiments for few-electron projectiles. A further comparison can be made for the "total" cusp cross section σ^{ELC} as determined by integration of $d\sigma/dv_e$ between $v_P-0.5$ and $v_P+0.5$. Figure 15 shows the experimental and theoretical σ^{ELC} for O^{5+} and O^{4+}. Although only poorly justified in a Be-like configuration, we use a hydrogenic approximation also for O^{4+}. The experimental energy dependence can be well reproduced for both systems whereas the absolute magnitude of σ^{ELC} is overestimated by a factor 1.5 or 2. The comparison of Figs. 14 and 15 suggest that the anisotropy (and therefore Γ) is less sensitive than the absolute cross section to both the simple approximation for the wave function and to the Born approximation a feature often observed in calculations for bound-state excitation.

For collisions of hydrogenic $O^{7+}(1s)$ projectiles, the calculation has failed to reproduce experimental data[5] for the cusp shape at $v_P=7.07$. The experimental width, $\Gamma_{\text{expt}} \lesssim 0.3$, is much smaller than predicted by the calculation, $\Gamma_{\text{theor}}=0.49$ (a rough estimate for Γ at $Z_P=8$ and $v_P=7.07$ can be taken from Figs. 9 and 11). More seriously, the data show an asymmetric cusp skewed to the low-velocity side similar to that for ECC. Since the data were taken in coincidence with the outgoing charge state, ECC should be ruled out as a major source of the asymmetry. The failure of the Born approximation is not surprising because of $v_P/v_{\text{orbital}}<1$ in this case. Furthermore, the ionization of the deeply bound $1s$ electron requires close collisions where the interaction with the argon nucleus is not small.

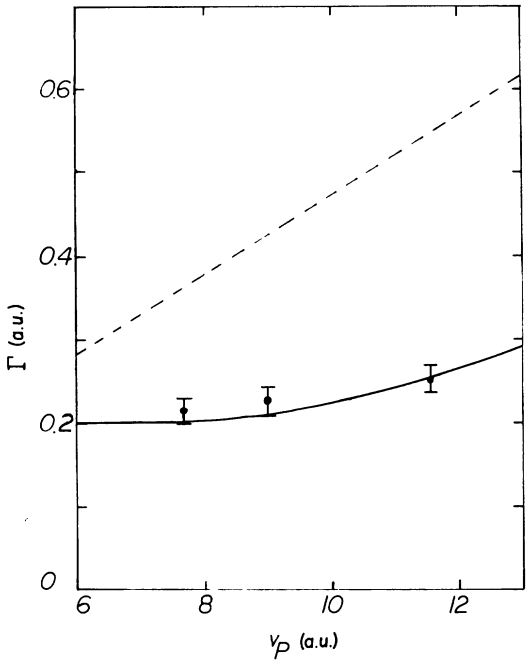

FIG. 14. ELC cusp width for O^{5+} on argon ($\theta_0=3.14\times10^{-2}$ rad $\cong 1.8°$) as a function of the projectile velocity; ——, present calculation; — — —, width for isotropic electron emission; ▮ experimental data (Ref. 5).

It is interesting to note the similarities and differences of the forward-backward asymmetry for ECC and ELC. As in the case of ECC (Ref. 34) we find that the asymmetry of the DDCS is a signature of the presence of higher-order Born terms. There is, however, a remarkable difference: In the limit of asymptotic projectile velocities $v_P \gg 1$ the DDCS asymmetry persists for ECC (Ref. 35) because of the dominance of the second-order Born contri-

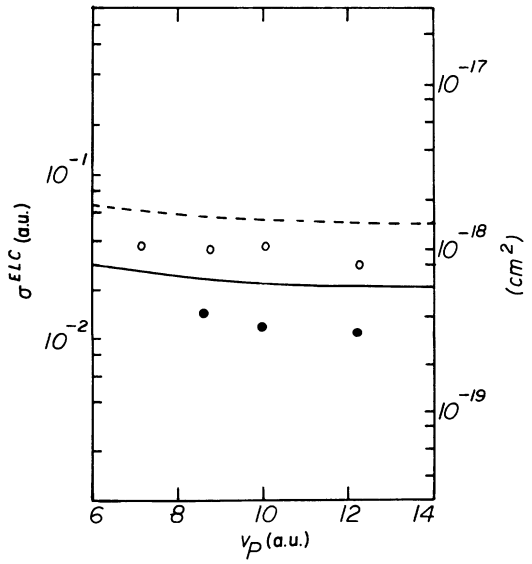

FIG. 15. Integrated absolute ELC cusp cross sections (see text) for O^{q+} argon as function of the projectile velocity v_P. Present theory: ——, $q=5$; ——, $q=4$; experiment (Ref. 5): ●, $q=5$; ○, $q=4$.

bution[36] whereas for ELC the DDCS should become symmetric because the first-order Born approximation is believed to be the leading term of the perturbation expansion for large v_P (Ref. 14) (although a conclusive proof is not yet available).

One further aspect deserves attention for hydrogenic projectiles: The O^{7+} beam contains, after leaving the stripper foil, an admixture of metastable $O^{7+}(2s)$ projectiles. The detected cusp is then a superposition of ELC contributions of the $1s$ and $2s$ initial states. Our present results emphasize the importance of even small admixtures of metastables because of the large $2s$ ELC cross section in the cusp region. Assuming an admixture of 3% metastables[37] we find under the same experimental conditions as discussed above a reduction of the calculated width from $\Gamma=0.49$ to 0.35. Therefore, more accurate measurements of the $1s$ ELC cusp shape should be performed in future by quenching the $2s$ state before entering the collision region.

VII. CONCLUSIONS

We have shown that a well-known group-theoretical O(4,2) approach for calculating bound-bound transitions in hydrogenic systems can be easily extended to bound-free transitions in the limit of low-lying continuum states using the continuity across the ionization limit. The method yields a relatively simple closed expression for the triply differential cross section for projectile ionization of an arbitrary initial state $|n,l,m\rangle$. The doubly differential and the single differential cross section can be found by a one-dimensional numerical integration over the transverse momentum transfer. The angular distribution of the DDCS or TDCS becomes increasingly anisotropic with larger principal quantum number n.

The results have been used for a systematic investigation of the cusp shape for electron loss to continuum as a function of the initial state of the released electron. We have found a variety of possible shapes including a very narrow cusp for a $2s$ state and an inverted cusp for a $2p_0$ state. The strong dependence on the initial state contrasts with a weak dependence on the projectile velocity, the binding energy of the released electron, and the target. The calculated cusp width shows good qualitative (and sometimes quantitative) agreement with data concerning electron loss from the $n=2$ level of highly charged ions. Discrepancies for K-shell ionization are very likely linked with the failure of the Born approximation in the energy region where projectile and orbital velocity are of the same order of magnitude.

ACKNOWLEDGMENTS

This work was supported by National Science Foundation, by the Fundamental Interactions Branch, Division of Chemical Sciences, Office of Basic Energy Sciences, U.S. Department of Energy, under Contract No. W-7405-eng-26 with Union Carbide Corporation; and by the Deutsche Forschungsgemeinschaft (Sonderforschungsbereich 161).

APPENDIX A

In this appendix we summarize the basic ideas and the final result for the algebraic O(4,2) calculation[8] of the bound-bound transition form factor of hydrogen.

The method is based on the fact that the hydrogenic Schrödinger equation in parabolic coordinates (ϵ,η,ϕ) can be transformed into a Schrödinger equation for two two-dimensional harmonic oscillators with identical quantum-number–dependent oscillator frequencies

$$\omega_n = Z_P/n \ . \tag{A1}$$

One can therefore establish a one-to-one correspondence between the parabolic quantum numbers (n_1,n_2,m) and those for the oscillators (s,m) and $t,m)$:

$$s=2n_1+|m|+1 \ , \quad t=2n_2+|m|+1 \ , \tag{A2}$$

$$s+t=2n \ . \tag{A3}$$

The Lie invariance algebra connected with the group degeneracy within an n shell is O(4).[38] In the oscillator representation, transitions between states with different quantum numbers ($s\rightarrow s'$ or $t\rightarrow t'$) can be described by the usual oscillator creation or destruction operators. By incorporating quadratic forms of the oscillator shift operators, the O(4) algebra can be extended to the O(4,2) noninvariance algebra whose irreducible representation space is the complete oscillator Hilbert space. The elements of O(4,2) allow an algebraic description of transitions between all oscillator states. According to the correspondence to the hydrogenic Schrödinger equation, the O(4,2) algebra permits an algebraic description of n-changing transitions in the physical bound-state Hilbert space provided we adjust the n dependent oscillator frequencies [see Eqs. (A1) and (A3)]. The rescaling of ω_n can be done with help of a scaling operator S which is itself an element of the group generated by exponentiation of the O(4,2) Lie algebra. Consequently, bound-bound transitions can be described in a completely algebraic way. We quote here the final result for the transition form factor as given by Englefield[8] adopted to our present notation:

$$\langle n',n_1',n_2',m\,|\,e^{iQz}\,|\,n,n_1,n_2m\rangle$$
$$=(-1)^{n_1'+n_2}\frac{K}{2}\left[\frac{(n_1'+|m|)!(n_2'+|m|)!(n_1+|m|)!(n_2+|m|)!}{n_1'!n_2'!n_1!n_2!}\right]^{1/2}$$
$$\times\left[\frac{4nn'}{(n+n')^2+K^2n^2(n')^2}\right]^{|m|+2}\frac{(n-n'-iKnn')^{n_1+n_2'-1}(n-n'+iKnn')^{n_1'+n_2-1}}{|m|!^2(n+n'-iKnn')^{n_1+n_1'}(n+n'+iKnn')^{n_2+n_2'}}$$

$$\times[\{2Kn^2(n')^2+2inn'(n_2-n_1)+i[n^2+(n')^2+K^2n^2(n')^2](n_1'-n_2')\}$$

$$\times {}_2F_1(-n_1,n_1',|m|+1,y)\,{}_2F_1(-n_2,n_2',|m|+1,y)$$

$$+i[(n+n')^2+K^2n^2(n')^2][n_2'\,{}_2F_1(-n_1,-n_1',|m|+1,y)\,{}_2F_1(-n_2,-(n_2'-1),|m|+1,y)$$

$$-n_1'\,{}_2F_1(-n_1,-(n_1'-1),|m|+1,y)\,{}_2F_1(-n_2,-n_2',|m|+1,y)]] . \quad \text{(A4)}$$

In (A4) we have introduced the following abbreviations:

$$K=Q/Z_P , \quad \text{(A5a)}$$

$$y=-4nn'[(n-n')^2+K^2n^2(n')^2]^{-1} . \quad \text{(A5b)}$$

It is important to note that the scaling operator maps the complete oscillator Hilbert space into the subspace of hydrogenic bound states. Therefore, (A4) cannot directly be applied to transitions into the hydrogenic continuum. An extension is, however, possible via analytic continuation. In Sec. IV, we discussed a very simple method for inclusion of low-lying continuum states by calculating the Rydberg limit $n'\to\infty$ of (A4) and using the continuity across the ionization limit.

---

*On leave of absence from Institut für Atom- und Festkörperphysik, Freie Universität Berlin, D-1000 Berlin 33, West Germany.

[1]A Salin, J. Phys. B 2, 631 (1969).

[2]J. Macek, Phys. Rev. A 1, 235 (1970).

[3]F. Drepper and J. S. Briggs, J. Phys. B 9, 2063 (1976); J. S. Briggs and F. Drepper, *ibid.* 11, 4033 (1978); J. S. Briggs and M. H. Day, *ibid.* 13, 4797 (1980); M. H. Day *ibid.* 13, L65 (1980); 14, 231 (1981).

[4]R. Cranage, W. Steckelmacher, and M. Lucas, Nucl. Instrum. Methods 194, 419 (1982).

[5]M. Breining, S. B. Elston, S. Huldt, L. Liljeby, C. R. Vane, S. D. Berry, G. A. Glass, M. Schauer, I. A. Sellin, G. D. Alton, S. Datz, S. Overbury, R. Laubert, and M. Suter, Phys. Rev. A 25, 3015 (1982).

[6]For sake of brevity we use for both $T(n,l,m\to\vec{v},\vec{Q})$ and $|T(n,l,m\to\vec{v},\vec{Q})|^2$ the term transition form factor.

[7]L. C. Biedenharn, J. Math. Phys. 2, 433 (1961).

[8]M. J. Englefield, *Group Theory and the Coulomb Problem* (Wiley-Interscience, New York, 1972). See also A. O. Barut and H. Kleinert, Phys. Rev. 157, 1080 (1967); 160, 1149 (1967).

[9]K. Omidvar, Phys. Rev. 140, A26 (1965).

[10]Dz. Belkić, J. Phys. B 14, 1907 (1981).

[11]M. R. C. McDowell and J. P. Coleman, *Introduction to the Theory of Ion-Atom Collisions* (North-Holland, Amsterdam, 1970), p. 210.

[12]J. G. Lodge, J. Phys. B 2, 322 (1969).

[13]J. Burgdörfer, J. Phys. B 14, 1019 (1981).

[14]J. Briggs, J. Macek, and K. Taulberg, Comments At. Mol. Phys. XII, 1 (1982).

[15]A. K. Kaminski and M. I. Popova, J. Phys. B 15, 403 (1982).

[16]M. E. Rudd and J. Macek, Case Stud. At. Phys. 3, 47 (1972).

[17]K. Knopp, *Elements of the Theory of Functions* (Dover, New York, 1952), p. 36.

[18]H. A. Bethe and E. E. Salpeter, *Quantum Mechanics of One- and Two-Electron Atoms* (Springer, Berlin, 1957), p. 29.

[19]W. Magnus, F. Oberhettinger, and R. P. Soni, *Formulas and Theorems for the Special Functions of Mathematical Physics* (Springer, New York, 1966), p. 245.

[20]*Formulas and Theorems for the Special Functions of Mathematical Physics,* Ref. 19, p. 107.

[21]E. P. Wigner, Phys. Rev. 73, 1002 (1948).

[22]W. Meckbach, I. B. Nemirovski, and C. R. Garibotti, Phys. Rev. A 24, 1793 (1981).

[23]J. Burgdörfer, Z. Phys. A 309, 285 (1983).

[24]E. P. Wigner, *Group Theory* (Academic, New York, 1959), p. 351.

[25]A. Messiah, *Quantum Mechanics* (North-Holland, Amsterdam, 1970), Vol. 2, p. 1073.

[26]In order to be consistent with Ref. 8, we choose in Eq. (27) a phase convention slightly different from our earlier work (Ref. 23). There, we have included the familiar phase factor for the spherical harmonics, $(-1)^m$ for $m>0$, into the definition of the parabolic wave functions. In Eq. (27) we use the standard definition of Ref. 8.

[27]A. Gaupp, H. J. Andrä, and J. Macek, Phys. Rev. Lett. 32, 268 (1974).

[28]*Introduction to the Theory of Ion-Atom Collisions,* Ref. 11, p. 334.

[29]N. Maleki and J. Macek, Phys. Rev. A 26, 3198 (1982).

[30]J. H. Hubbell, W. J. Veigele, E. A. Briggs, R. T. Brown, D. T. Cromer, and R. J. Howerton, J. Phys. Chem. Ref. Data 4, 471 (1975).

[31]K. Omidvar and H. Lee Kyle, Phys. Rev. A 2, 408 (1970).

[32]J. Burgdörfer, Phys. Rev. Lett. 51, 374 (1983).

[33]K. Dettmann, K. G. Harrison, and M. W. Lucas, J. Phys. B 7, 269 (1974).

[34]R. Shakeshaft and L. Spruch, Phys. Rev. Lett. 41, 1037 (1978); J. Macek, J. E. Potter, M. M. Duncan, M. G. Menendez, M. W. Lucas, and W. Steckelmacher, *ibid.* 46, 1571 (1981).

[35]S. D. Berry, I. A. Sellin, K. O. Groeneveld, D. Hoffmann, L. H. Andersen, M. Breinig, S. B. Elston, M. M. Schauer, N. Stolterfoht, H. Schmidt-Böcking, G. Nolte, and G. Schiwietz, IEEE Trans. Nucl. Sci. NS-30, 902 (1983).

[36]R. Shakeshaft and L. Spruch, Rev. Mod. Phys. 51, 369 (1979).

[37]M. Leventhal, Nucl. Instrum. Methods 110, 343 (1973).

[38]V. Fock, Z. Phys. 98, 145 (1935).